Scanning Microscopy

Volume 3 | Number 3 Article 12

6-7-1989

Recent Uses of Electron Microscopy in the Study of Physico-Chemical Processes Affecting the Reactivity of Synthetic and Biological Apatites

J. D. B. Featherstone
Eastman Dental Center

D. G. A. Nelson
Victoria University of Wellington

Scanning Microscopy, Vol. 3, No. 3, 1989 (Pages 815-828)
Scanning Microscopy International, Chicago (AMF O'Hare), IL 60666 USA

0891-7035/89$3.00+.00

RECENT USES OF ELECTRON MICROSCOPY IN THE STUDY OF PHYSICO-CHEMICAL PROCESSES AFFECTING THE REACTIVITY OF SYNTHETIC AND BIOLOGICAL APATITES

J.D.B. Featherstone[1]* and D.G.A. Nelson[2]

[1]Department of Oral Biology, Eastman Dental Center,
625 Elmwood Avenue, Rochester, NY 14620, USA; and

[2]Electron Microscope Facility, Victoria University of Wellington, New Zealand
Present address: Proctor & Gamble, Miami Valley Labs., Cincinnati, OH 45239

(Received for publication September 15, 1988, and in revised form June 7, 1989)

Abstract

Studies which used scanning electron microscopy (SEM) to investigate subsurface demineralization of dental enamel have recently been well reviewed. The purpose of the present paper was to review several studies, carried out in our laboratories, which have used electron microscopy to examine physicochemical properties of synthetic and biological apatites, to relate these results to previous studies, and to present new data.

Aspects of the ultrastructure of hydroxyapatite and carbonated-apatites have been observed by high resolution transmission electron microscopy, and related to shape and growth of these crystals.

Surface morphologies of discs prepared from precipitated carbonated-apatites and from ceramic carbonated-apatites were examined by SEM and the information was used in the interpretation of apatite dissolution studies relevant to dental caries.

Improvements in the technique of backscattered electron imaging of demineralized enamel have enabled better interpretation of enamel caries experiments.

SEM examination of enamel and dentin treated by low energy lasers of specific wavelengths have shown that lasing conditions can be chosen that produce surface fusion of the apatite which inhibits caries-like lesion progression.

SEM examination of crystals formed on and in enamel during high concentration fluoride treatments implies that calcium fluoride-like crystals are formed and they may act as a slow-release fluoride reservoir in the mouth.

KEY WORDS: Scanning electron microscopy, dental enamel, apatite, carbonated apatite, laser, caries, ceramic apatite.

* Address for Correspondence:
J.D.B. Featherstone,
Department of Oral Biology, Eastman Dental Center,
625 Elmwood Avenue,
Rochester, NY 14620, USA,
Phone No. (716) 275-5015

Introduction

Scanning electron microscopy (SEM) has been frequently used to study the morphology of acid or ethylenediaminetetraacetic acid (EDTA) etched enamel surfaces. The demineralization of enamel that occurs during subsurface caries lesion formation has also been extensively studied and pore sizes and crystal diameters have been measured. These studies have been thoroughly reviewed recently by Shellis and Hallsworth (1987). However, there are several other physicochemical processes of importance in the dentally-relevant field that modify the surface morphology considerably. Some of these processes, including the use of topical fluoride applications and the use of infrared laser radiation, are either currently used or have potential uses as caries-preventative methods. The purpose of the present paper is to review and bring together several of these studies carried out in our laboratories, to demonstrate their relationship to the understanding of dental caries, to relate these results to previous studies, and to present new data.

Ultrastructure and shape of apatite crystals

The crystalline phase in biological mineralized tissues such as bone and dental enamel approximates the crystal structure of the minerals hydroxyapatite, [$Ca_{10}(PO_4)_6(OH)_2$, (HAP)] and fluorapatite, [$Ca_{10}(PO_4)_6F_2$, (FAP)] (Simpson, 1972; Young, 1974). The crystal structure of FAP belongs to the hexagonal system and has a space group, $P6_3/m$. Most preparations of HAP also show hexagonal symmetry, but the space group $P6_3/m$ is probably correct only for materials stabilized by impurities and vacancies in the hexad axis which contains a column of X ions where X = F, OH (Kay et al., 1964). A monoclinic form of apatite has been reported where the X columns of OH groups are alternatively orientated up and down (Elliott et al., 1973), but they have only been prepared at high temperatures and probably have little relevance to the crystal structure of biological apatites which are nonstoichiometric and contain up to 5 percent carbonate. When the generic apatite crystal structure which serves as the base model for biological apatites is projected in the c-axis direction it has a hexagonal symmetry. When HAP crystals are examined by high resolution transmission electron microscopy (TEM) and oriented parallel to their c-axes in the [001] zone axis, sub-unit cell detail with mainly hexagonal symmetry can be

directly visualized (Fig. 1). This detail can be compared with corresponding projections of the apatite crystal structure and with computer-simulated lattice images and in the best cases, a direct correspondence between the sites of calcium atoms and phosphate groups and detail in the images has been achieved (McLean and Nelson, 1982; Nelson et al., 1983a; Nelson and McLean, 1984b; Bres et al., 1985). HAP crystals oriented parallel to their b-axes in their [010] zone axis, exhibit images with orthorhombic symmetry and the rectangular outline of the projected unit cell has been marked in white in the image (Fig. 2). The [011] zone axis orientation is also a commonly used orientation for high resolution TEM of apatite crystals (Bres et al., 1985).

The shape of the crystals that initially nucleate in mineralizing enamel appear to be long thin ribbons that bend and twist and have edges that sometimes appear to be folded over onto the ribbon (Nylen et al., 1963; Frazier, 1968). As the initial crystals grow laterally, they develop flattened hexagonal cross-sections approximately 15-50 nm thick and 40-100 nm wide that have been observed by TEM (Kerebel et al., 1979). Although an apatite-like material is the end product of the mineralization process, it is possible that the formation of these apatites from solutions that are initially very highly supersaturated, will proceed via intermediate precursor phases such as amorphous calcium phosphate and octacalcium phosphate (Brown et al., 1962; Brown et al., 1979), which often have only a transitory existence (Nancollas and Tomazic, 1974; Nancollas, 1982). In this context we used high resolution TEM to follow crystal-structural changes that occurred when octacalcium phosphate was hydrolyzed to form calcium deficient apatites (Nelson and McLean, 1984a) and found examples of intergrowths of the two materials.

Some investigators have suggested recently that biological apatite crystals have rectangular or rhombohedral cross-sections (Warshawsky et al., 1987; Warshawsky, 1987). While an apatite crystal with a rhombohedral cross-section with 60 or 120 degree internal angles is not at variance with the hexagonal symmetry of apatite, it is hard to see how a synthetic carbonated-apatite crystal such as the one in Fig. 3 does not have an approximately hexagonal cross-sectional shape. In this lattice image, the fine detail has a hexagonal symmetry because the crystal is oriented in the [001] zone axis (i.e., parallel to the apatite c-axis). The only possibility that the hexagonal outline does not reflect the true cross-section of the crystal is if the crystallographic c-axis is not parallel to the long axis of the crystal but significantly inclined to it. If this were the case, then images of apatite crystals projected parallel to the b-axis would show terminating (100) 0.82 nm fringes down the length of the crystals. For this and other crystallographic reasons we believe the evidence firmly supports the existence of flattened hexagonal cross-sectional shapes at least for relatively mature crystals.

Transmission electron micrographs of crystals in human dental enamel frequently have an electron-lucent or electron-opaque line in their centers (Frazier, 1968). While there have been many explanations for this feature it is now generally accepted that this feature is caused by a central planar defect in these biological crystals (Marshall and Lawless, 1981; Rachinger et al., 1982; Nakahara and Kakei, 1983; Bres et al., 1984). In order to gain some insight into the atomic scale structure of these planar defects we were able to prepare and examine synthetic apatites which had central planar defects (Fig. 4) (Nelson et al., 1986a). Using a variety of techniques, we determined that these synthetic defects were the result of a planar octacalcium phosphate inclusion, often one unit cell thick, embedded in, and surrounded by an apatite matrix. This suggests that a unit cell thick plate of octacalcium phosphate is the critical crystal nucleus that acts as a template for further apatite growth. Therefore, in some conditions octacalcium phosphate appears to be involved in the nucleation of apatite crystals and these initial crystal nuclei may not yet have flattened hexagonal cross-sectional outlines.

Figure 1 (on the facing page). High resolution lattice image of a synthetic stoichiometric hydroxyapatite crystal oriented in the [001] zone axis. Insert shows the corresponding electron diffraction pattern and a projection of the apatite unit cell is marked in white.

Figure 2 (on the facing page). High resolution lattice image and corresponding electron diffraction pattern of a synthetic stoichiometric hydroxyapatite crystal oriented in the [010] zone axis. The projected apatite unit cell is marked in white.

Although up until the present time, most investigations of apatite crystal morphology have been done using TEM, new advances in SEM technology mean that the morphology of biological apatite crystals can be studied using this technique. The problem with SEM is that standard sputtered coatings of gold or platinum are usually 5-20 nm thick and obscure topographical detail of the crystal shape. This results in biological apatite crystals being observed as thin needle-like crystals with rounded ends, which they obviously are not. However, the use of uncoated specimens or specimens with very thin coatings (in the order of 1 nm thick) would appear to resolve these problems if sufficient resolution could be obtained using SEM. Recent preliminary studies on the shape of biological apatite crystals using a recently-developed high resolution field emission SEM have been very promising (Gantt and Guntekunst, 1988). Recent studies by LeGeros and coworkers have shown similar results (LeGeros and LeGeros, personal communication).

Apatite reactivity

Many physicochemical studies have been carried out using hydroxyapatite as a model substance in attempts to understand the reactivity of biological apatites. It is beyond the scope of the present paper to review these studies. Biological apatites, including dental enamel, are highly substituted apatites with carbonate being one of the major substituents (LeGeros, 1967; LeGeros, 1977). However, relatively few workers have used well-characterized carbonated-apatites as model materials to carry out studies related to dental caries. A recent study by Budz et al. (1987) clearly showed that synthetic carbonated-apatites (supplied from our laboratories) behaved more like dental enamel in constant composition experiments than did pure hydroxyapatite. We have used a specially constructed dissolution apparatus to

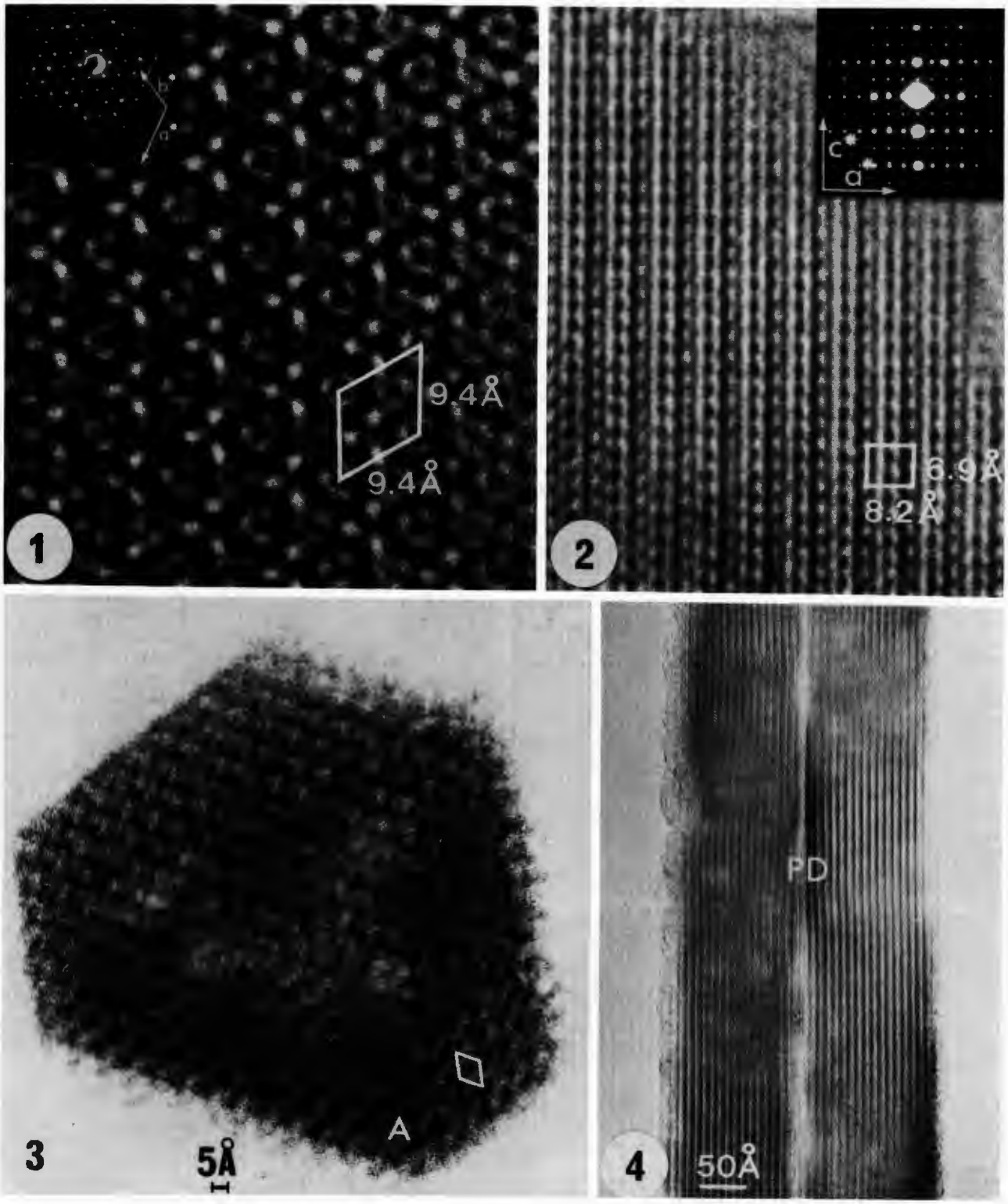

Figure 3. Lattice image of a synthetic precipitated carbonated-apatite crystal oriented in the [001] zone axis. Notice the hexagonal symmetry in region labelled A and the projected apatite unit cell marked in white.

Figure 4. Lattice image of a synthetic carbonated-apatite crystal oriented in the [011] zone axis with a central planar defect (labelled PD).

study the role of carbonate, fluoride, and other trace elements in apatite reactivity (Featherstone et al., 1983; Glena et al., 1984). One of the features of that previously reported system was that we used pressed pellets of synthetic carbonated-apatites made by aqueous precipitation. However, some intercrystalline diffusion still occurred and particle size made some contribution (Nelson et al., 1989). In order to study the possible inhibitory effect of salivary proteins and lipids on the surface dissolution of synthetic carbonated-apatites we have used ceramic carbonated-apatite discs in the apparatus (Kautsky, 1988). The discs were made in our laboratories by high-temperature sintering of discs prepared from precipitated carbonated-apatites and the procedure is fully described elsewhere (Ellies et al., 1988a). In brief, precipitated carbonated apatites were sintered at 900-1000°C in a moist carbon dioxide atmosphere for periods of 2-4 hours. Typically, up to 30 percent of the original carbonate content was lost during sintering. In all cases the final carbonate content was analyzed after sintering. In the present paper we report for the first time the comparison by SEM of the precipitated carbonated-apatites (Fig. 5), the surface of precipitated carbonated-apatite pressed into discs (Figs. 6 and 7) and the surface of the ceramic carbonated-apatite discs (Figs. 8, 10 and 11).

The high magnification (Fig. 7) inspection of the pressed precipitated-apatite discs showed a surface morphology somewhat similar to that of normal enamel at the crystalline level (Fig. 9). The crystals were of similar diameter and intercrystalline spaces were available for diffusion of chemical species into the pellet. The ceramic apatites were shown to be essentially non-porous with the surface holes not continuing inward and the crystals having fused into one surface (Figures 9 and 10) without intercrystalline pores. The highly crystalline nature of the material was confirmed by sharp X-ray diffraction patterns similar to those of dental enamel (Ellies et al., 1988a). Adsorption of parotid or whole saliva in vitro or in vivo onto these discs produced up to 70 percent inhibition of dissolution during subsequent acid challenge in our dissolution apparatus (Kautsky, 1988), demonstrating the high degree of protection provided to apatite surfaces by salivary components. Studies are ongoing to determine which salivary proteins and/or lipids provided this protection.

Dissolution experiments in our laboratories using the pressed disc model (Nelson et al., 1983c; Glena et al., 1984) showed that the primary effect of fluoride in dissolution inhibition was when it was present in the acid buffer during the challenge to the carbonated-apatite. The reduction in dissolution rate was proportional to the logarithm of the fluoride concentration.

Biocompatibility studies using ceramic carbonated apatites prepared as described above (Ellies et al., 1988a) showed this material to have excellent potential as a dental implant material (Ellies et al., 1988b).

Backscattered electron imaging of demineralized enamel

One of us has been using backscattered electron (BSE) imaging in the SEM to study the extent of demineralization in natural and artificial caries lesions (Nelson and Pearce, 1988; Pearce and Nelson, 1989). Using this technique it is possible to obtain subsurface compositional details that reflect variations in enamel mineral density. Although images of subsurface lesions were obtained using BSEs many years ago (Boyde et al., 1961), it was not until the advent of the more efficient, solid-state, wide-angle, 4-quadrant BSE detector that this technique has been used again recently in the study of lesion formation.

Jones and Boyde (1987) recently reported that the BSE imaging technique offered a significant improvement in resolution to previously used techniques for investigating the extent of demineralization in caries-like lesions in dental enamel. We have also found this to be the case and, in addition, have obtained new information about the de- and remineralization processes that occur during subsurface lesion formation. This information could not be obtained using the standard techniques of polarized light microscopy, microradiography or microhardness testing.

Two different types of specimen preparation were used by us to produce BSE images of demineralized enamel. The first preparative technique consisted of serially-polishing (down to 1 micrometer diamond paste) the anatomical surface of enamel chips and then producing caries-like lesions on these surfaces, either by exposing them to acidic demineralizing solutions under pH cycling conditions (Featherstone et al., 1986) or to in vivo conditions in an intra-oral caries device. After various time periods, the polished surfaces which were either surface softened or had subsurface lesions were examined using SEM. This technique produced images of the prism structure in cross-section (Figs. 12, 13) where the prism peripheries were more highly mineralized than the prism cores. These results are more fully described and discussed elsewhere (Pearce and Nelson, 1989). Calculations using Monte Carlo simulation techniques showed that at 30kV, the backscattered electrons resulted from scattering no deeper than 4 micrometers beneath the surface and therefore these images had a good depth of field. However, images of this type were limited to studying

Figure 5. Precipitated carbonated-apatite (approximately 3 percent carbonate) as used in pressed disc preparation for dissolution studies. Bar = 100 nm.

Figure 6. Unpolished surface of pressed pellet prepared from precipitated carbonated-apatite. Bar = 100 micrometers.

Figure 7. Higher magnification SEM of pellet surface shown in figure 6. Bar = 100 nm.

Figure 8. Low magnification SEM of polished surface (0.05 micrometer alumina) of a ceramic carbonated-apatite disc. Bar = 100 micrometers.

Figure 9. Higher magnification SEM of a normal enamel surface showing somewhat similar appearance to the pressed precipitated apatite disc surface. Bar = 100 nm.

Figure 10. Higher magnification SEM of surface of a ceramic carbonated-apatite (6 percent carbonate) shown in Figure 8. Bar = 1 micrometer.

Figure 11. Higher magnification SEM of surface of a ceramic carbonated-apatite (3 percent carbonate). Bar = 1 micrometer.

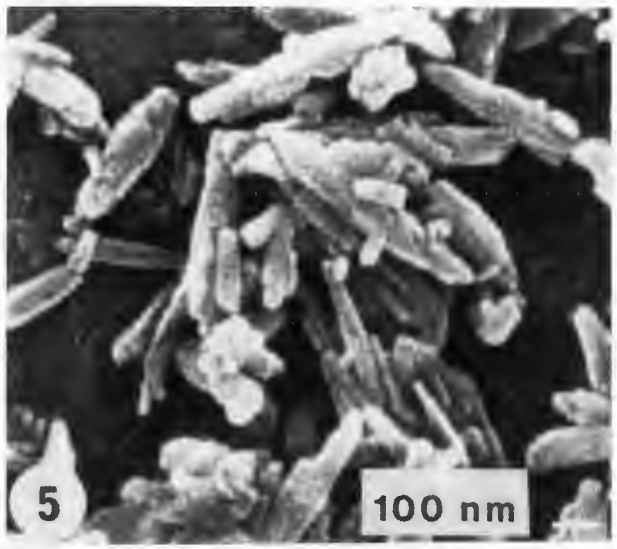
5
100 nm

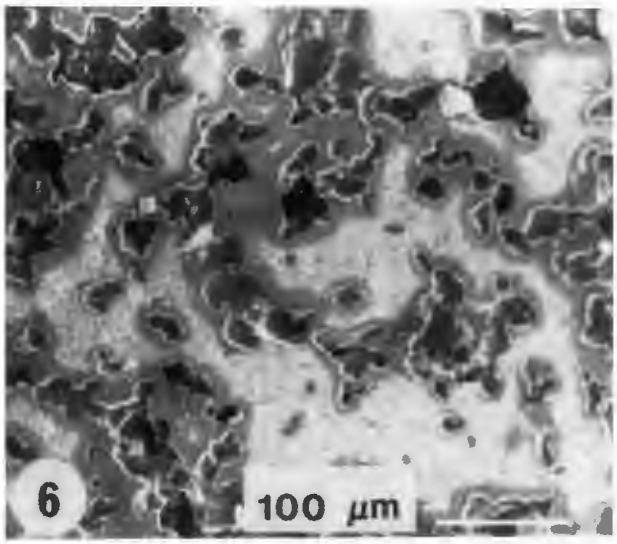
6
100 μm

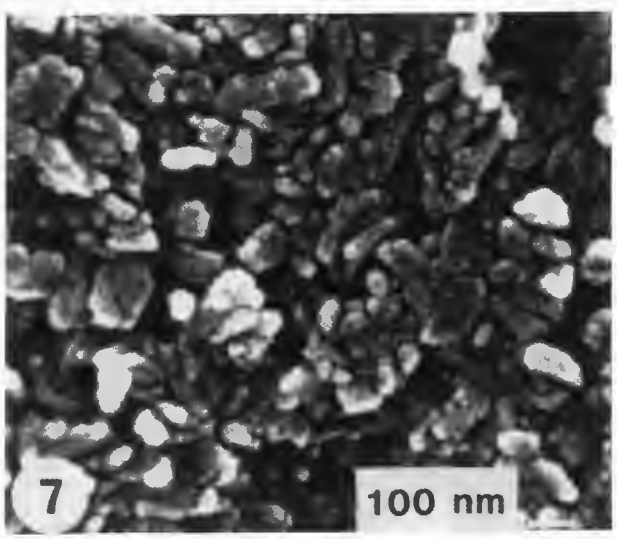
7
100 nm

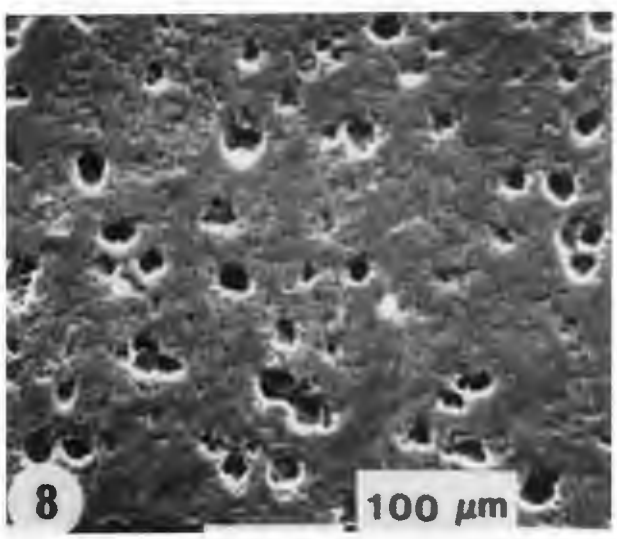
8
100 μm


9
100 nm

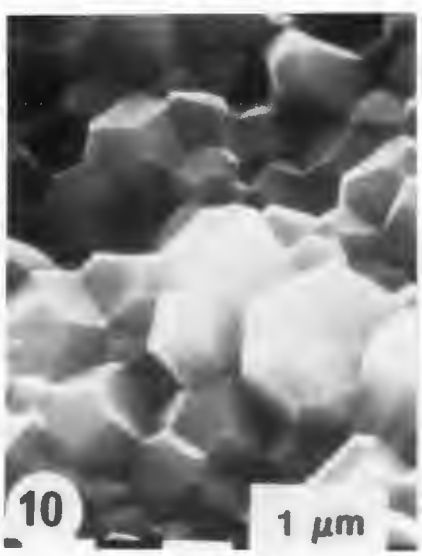
10
1 μm

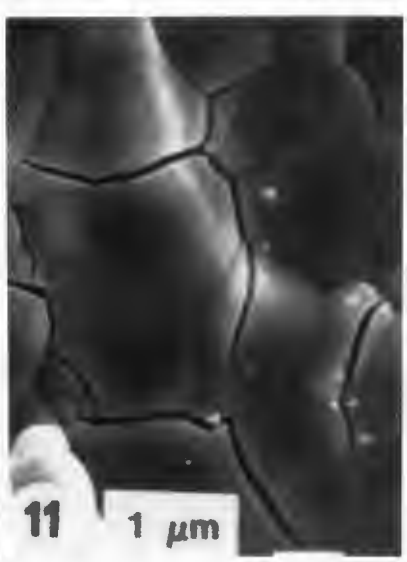
11
1 μm

demineralization in the immediate surface layer of the lesion because of the shallow depth that backscattered electrons originated from. The second preparative technique involved transversely sectioning an enamel specimen with a caries-like lesion, serially polishing one of the cut faces, and examining the polished surface using BSE imaging to get a transverse image of the lesion similar to those obtained using microradiography or polarized light microscopy (Figs. 14-17). Figures 14, 15 show a 25 micrometers lesion produced in an intra-oral caries device, whereas figures 16, 17 show a 140 micrometers laminated lesion produced artificially using a pH cycling regime.

In both the cross-sectional and longitudinal images we observed several interesting phenomena:

(1) At the advancing front of the lesions, at the so-called translucent zone observed when using polarized light microscopy, prism peripheries demineralized first giving a "picket fence" appearance.

(2) In the body of the lesions the prism cores demineralized significantly, but the prism peripheries now had a greater mineral density than the cores, suggesting remineralization had occurred in these regions.

(3) In the zone between the advancing front of the lesion and the body of the lesion at what has been called the dark zone, a zone which shows features of remineralization (Silverstone, 1977), cores of the prisms sometimes had a greater mineral density than prisms in intact enamel while prism peripheries were demineralized (labelled r, Figs. 14, 15).

(4) In cross-sectional images especially, the cores of the prisms did not demineralize evenly and often small regions of greater mineral density in the center of partially demineralized prism cores were observed (large white arrow, Fig. 12). The non-uniform demineralization of prism cores in the body of the lesion was often related to features with alternating variations in mineral density called cross-striations that were spaced relatively regularly 3-5 micrometers apart.

BSE imaging is an excellent technique for visualizing microstructural details in demineralized enamel surfaces that have very little surface topography. It has a very good spatial resolution of approximately 0.1 micrometer, has a small depth of field with no adverse summation effects like polarized light and microradiography, where information in the image is summed over the 50-100 micrometers thickness of the section.

Enamel surfaces treated with pulsed laser radiation

Recent work by our group (Nelson et al., 1986b; Nelson et al., 1986c; Nelson et al., 1987; Featherstone and Nelson, 1987) has shown that low energy-density laser pulses at specific wavelengths in the infrared region are efficient in reducing acid dissolution of enamel and partially inhibiting artificial caries formation. We have found many factors, including the pulse energy density, the pulse interaction time and the wavelength of the laser radiation, to be important in influencing the morphology, reactivity and crystallography of lased enamel surfaces.

High energy density laser pulses (in the order of 10^4 J.cm^{-2}) produce deep fused pits in enamel surfaces and such high energies could seriously damage soft oral tissues, the pulp, or cause excessive cracking in the enamel. Pulses of lower energy densities, between 10-50 J.cm^{-2}, cause little damage to soft tissues or the pulp but are effective in inhibiting artificial caries formation. Pulse interaction times are also important because decreasing the pulse interaction time while keeping the pulse energy density constant increases the peak power density. Short pulses with interaction times of 100-200 ns, confine processes such as sintering, melting and recrystallization to a thin surface region without affecting the underlying enamel. Finally, the wavelength of the laser light used to irradiate the enamel surface is very important. Although dental enamel absorbs very little light in the visible region, it has intense absorption bands in the infrared region from 9.0-11.0 micrometers and consequently laser light from this region would be more efficiently absorbed than from other regions.

The surface morphology produced by a 400 pulse laser treatment of intact human enamel with a pulse energy density of 50 J.cm^{-2} at each of four different wavelengths was examined near the center of the irradiated areas using scanning electron microscopy (SEM) at magnifications ranging from 30 to approximately 11,000 times.

The 1073 cm^{-1} line produced a distinct surface melt on intact human enamel that at low magnifications (Fig. 18) exhibited extensive surface roughening which was more pronounced than the perikymata and may have been caused by preferential surface melting. At higher magnification (Fig. 19) the central melt region, although rough, was covered also by a thin smooth fused glaze-like surface layer that occasionally had broken away from the surface to reveal what appeared like a partially-fused mass of crystallites underneath the glaze-like surface layer.

The 1045 cm^{-1} line produced a surface melt morphology similar to that of the 1073 cm^{-1} line. At low magnifications in the center of the melt region (Fig. 20) considerable surface roughening occurred. At higher magnification, the central melt region, although rough, was covered by a thin smooth surface melt (Fig. 21).

The 973 cm^{-1} line produced a much less extensive area of surface roughening (Fig. 22) when compared to either of the 1073 and 1045 cm^{-1} lines.

Figure 12. BSE image of a polished, topographically flat, partially demineralized, enamel surface. Bar = 10 micrometers.

Figure 13. BSE image of a polished, topographically flat, partially demineralized, enamel surface. Bar = 10 micrometers.

Figure 14. BSE image of a longitudinal section through a 25 micrometers lesion formed in an intra-oral device. Bar = 10 micrometers.

Figure 15. Higher magnification of Fig. 14. Black arrows indicate demineralized prism peripheries. An area of remineralization is indicated by r. Bar = 10 micrometers.

Figure 16. BSE image of a longitudinal section through an artificial 140 micrometer laminated lesion formed by pH cycling. Bar = 100 micrometers.

Figure 17. Higher magnification of Fig. 16. Bar = 10 micrometers.

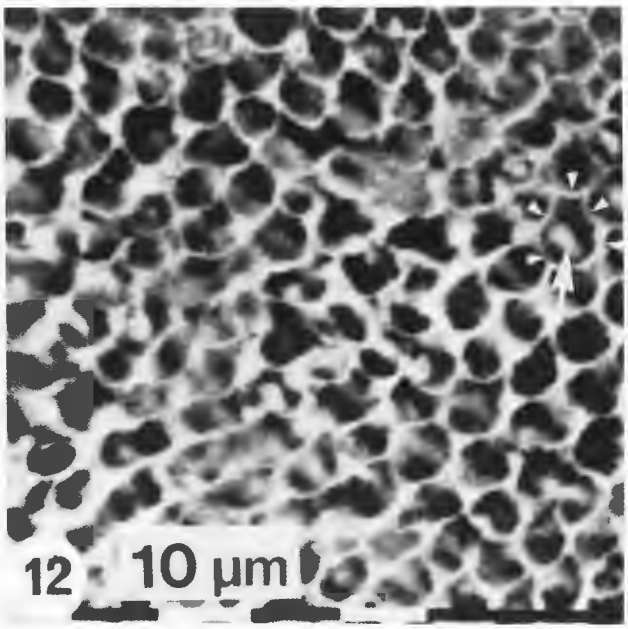
12
10 µm

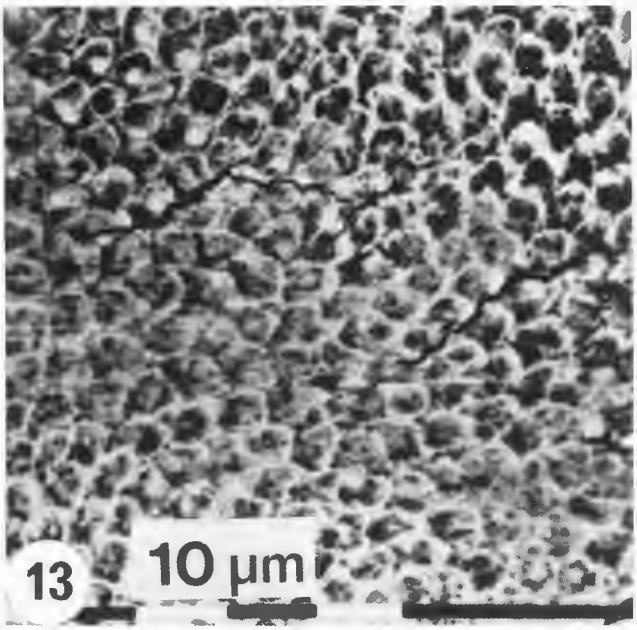
13
10 µm

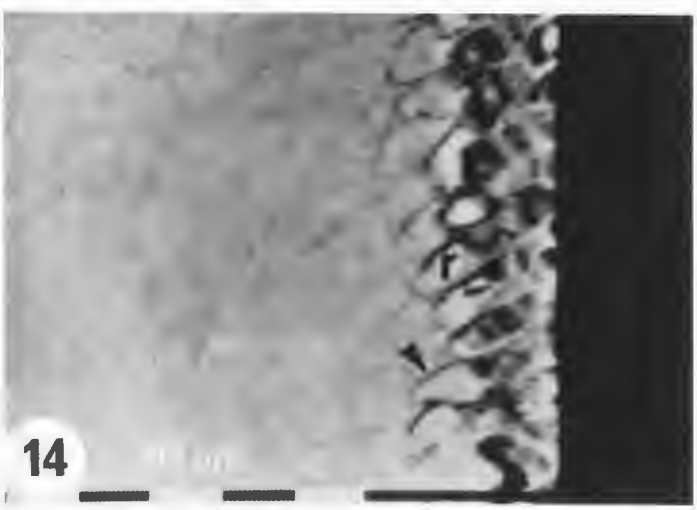
14

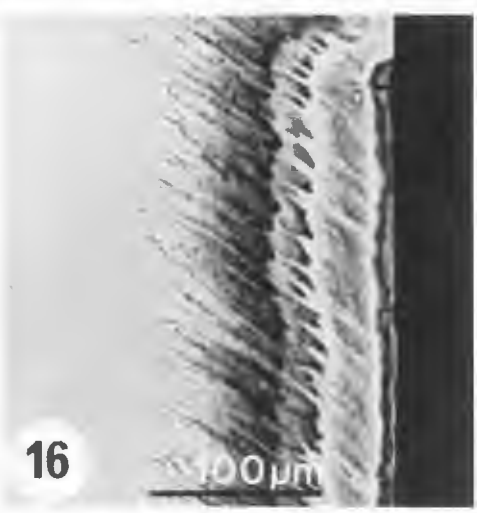
16

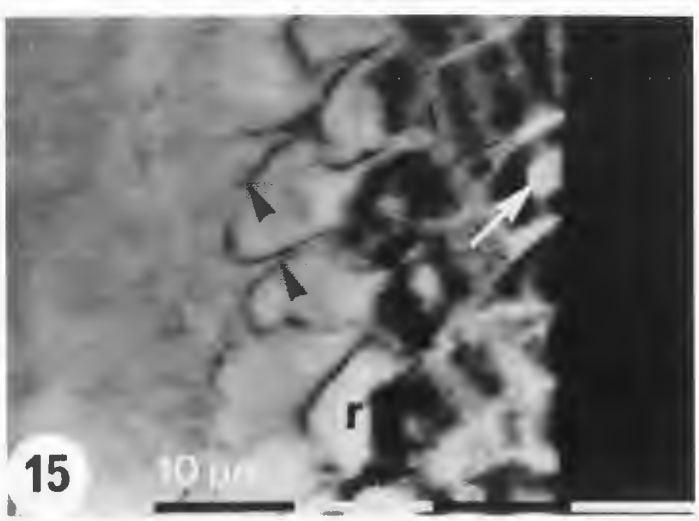
15
r

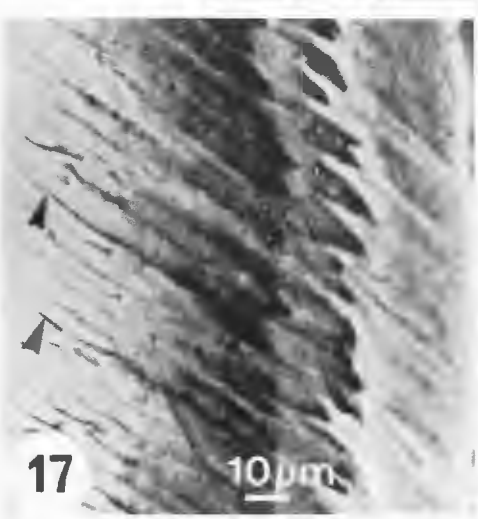
17
10 µm

The roughened area in the center of the melt zone was, however, similar in morphology to the corresponding regions of enamel irradiated with the 1073 and 1045 cm^{-1} lines both at low power (Fig. 22) and at higher power (Fig. 23).

Enamel irradiated with the 945 cm^{-1} line produced a melt zone characterized by hardly any surface roughening. At low magnification, for example, the perikymata were still visible transversing the irradiated area (Fig. 24). The central melt zone exhibited very little surface roughening and at higher magnification (Fig. 25) had the appearance of a smooth thin glaze-like surface melt covering the enamel surface.

Lased enamel surfaces that had been exposed to a lactate / diphosphonate demineralizing solution for up to 12 hours showed that the smooth, glaze-like surface rapidly broke down revealing etch patterns (Figs. 26-28) not consistent with normal dental enamel. Crystal morphologies distinctly different from enamel crystals were seen (Fig. 27). At greater magnifications (Fig. 28, arrows) some large crystals, approximately 0.5 micrometers in diameter, comprised part of the surface melt zone. Smaller crystals (less than 0.1 micrometers in diameter) were also seen.

These types of low-energy, pulsed, infrared laser pre-treatments of enamel and dentin strongly inhibited artificial lesion formation (Nelson et al., 1986c). Up to 50 percent inhibition of mineral loss was observed when sound enamel was pretreated with carbon dioxide laser radiation (1073 cm^{-1} line). In any future clinical applications where the laser would be used as a preventative measure, especially against fissure caries, the laser pre-treatments would be delivered using a fiber-optic device or some other directional device.

Human dentin that had been lased with a pulse energy density of 50 $J.cm^{-2}$ for 30 pulses at each of the four wavelengths produced very extensive surface roughening (Fig. 29) especially when compared with a control dentin surface (Fig. 32). Thin caps of fused material covering the tops of tag-like projections were observed (Figs. 30, 31) but did not appear to be related to the dentinal tubule structure (Fig. 32). Dentin roughened with this type of laser pre-treatment has been shown to enhance the bonding of composite resins to dentin (Cooper et al., 1988).

Enamel surfaces treated with topical fluoride agents

Topical fluoride agents normally consist either of acidic phosphate gels or varnishes with relatively high fluoride contents in the range of 0.1-2.5 wt. percent fluoride. The single application of a topical fluoride agent on dental enamel surfaces produces a thin (less than 1 micrometer) reaction product layer consisting mainly of a mixture of calcium fluoride-like (CaF_2) globules and some fluorapatite (FAP) crystals. Apart from the reaction product layer, fluoride is also incorporated into the enamel during application up to depths of 50 micrometers (Arends et al., 1984).

Using SEM, we investigated the morphologies of surface coatings produced by an acidulated phosphate fluoride (APF) gel containing 1.0 wt. percent as F, an acidic silane fluoride polyurethane-based varnish with the equivalent of 0.7 wt. percent as F (Fluor Protector) and a neutral NaF resinous varnish containing 2.26 wt. percent as F (Duraphat) (Nelson et al., 1983b). APF gel is widely used throughout the USA and Canada as a professionally-applied topical fluoride treatment. The neutral fluoride varnish is used in a similar way throughout Europe. Each agent reacted with the enamel surface differently, producing surface coatings of different thicknesses and different morphologies as well as producing its own distinctive etching pattern on the enamel surface.

Figure 18. SEM of intact human enamel lased at 1073 cm^{-1} with a pulse energy density of 50 $J.cm^{-2}$. Bar = 0.2 mm.

Figure 19. Higher magnification of Fig. 18 from the center of the lased area. Bar = 10 micrometers.

Figure 20. SEM of intact human enamel lased at 1045 cm^{-1} with a pulse energy density of 50 $J.cm^{-2}$. Bar = 0.2 mm.

Figure 21. Higher magnification of Fig. 20 from the center of the lased area. Bar = 10 micrometers.

Figure 22. SEM of intact human enamel lased at 973 cm^{-1} with a pulse energy density of 50 $J.cm^{-2}$. Bar = 0.2 mm.

Figure 23. Higher magnification of Fig. 22 from the center of the lased area. Bar = 10 micrometers.

Figure 24. SEM of intact human enamel lased at 945 cm^{-1} with a pulse energy density of 50 $J.cm^{-2}$. Bar = 0.2 mm.

Figure 25. Higher magnification of Fig. 24 from the center of the lased area. Bar = 10 micrometers.

Figure 26. SEM of enamel surface lased at 1073 cm^{-1} and exposed to a pH 5.0, 0.04 $mol.l^{-1}$ lactate / 0.1 $mmol.l^{-1}$ diphosphonate buffer for 12 hours,. Bar = 10 micrometers.

Figure 27. SEM of enamel surface lased at 1073 cm^{-1} and exposed to a pH 5.0, 0.04 $mol.l^{-1}$ lactate / 0.1 $mmol.l^{-1}$ diphosphonate buffer for 12 hours. Bar = 1 micrometer.

Figure 28. SEM of enamel surface lased at 1073 cm^{-1} and exposed to a pH 5.0, 0.04 $mol.l^{-1}$ lactate / 0.1 $mmol.l^{-1}$ diphosphonate buffer for 12 hours. Bar = 1 micrometer.

Figure 29. Typical SEM of dentin lased with 30 pulses at a pulse energy density of 50 $J.cm^{-2}$. Bar = 0.1 mm.

Figure 30. Higher magnification of Fig. 29. Bar = 50 micrometers.

Figure 31. Higher magnification of Fig. 30. Bar = 10 micrometers.

Figure 32. SEM of control dentin surface before lasing. Notice tubules are not related to the fused projections seen in Figs. 29-31. Bar = 5 micrometers.


18
0.2mm


19
10µm

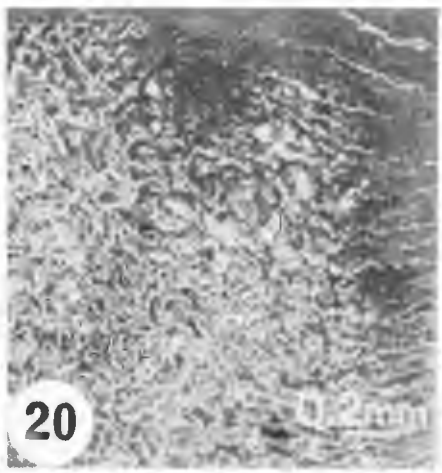
20
0.2mm


21
10µm

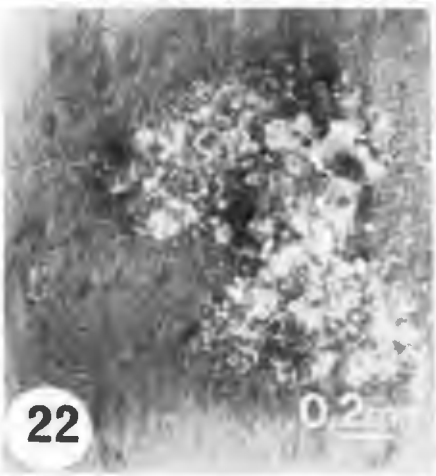
22
0.2mm


23

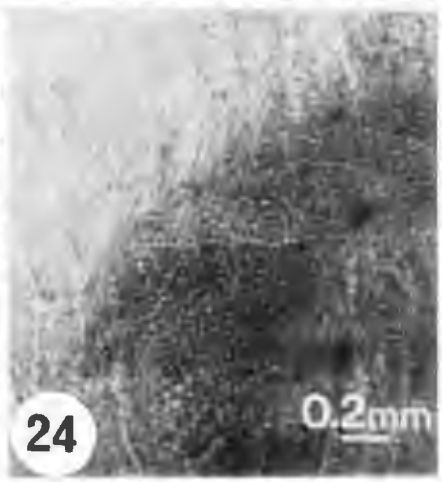
24
0.2mm

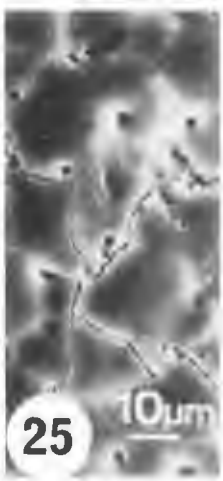
25
10µm

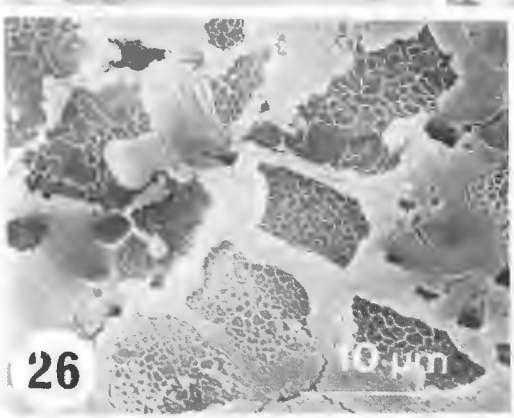
26
10µm

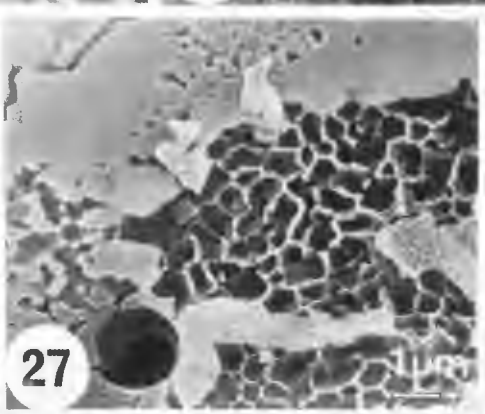
27


28

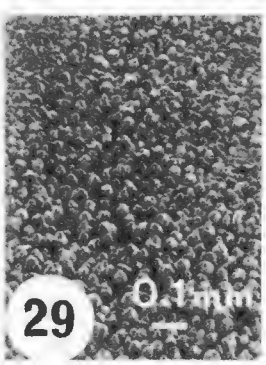
29
0.1mm

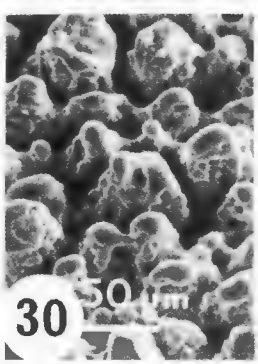
30
50µm

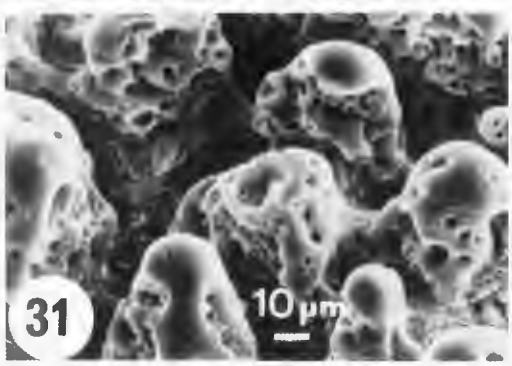
31
10µm


32
5µm

At low magnifications in the SEM spherical globules ranging from 0.3-3 micrometers in diameter (Figs. 33, 34) were observed. At higher magnifications the smallest particles observed in the surface coatings were approximately 20-30 nm in diameter, including the gold coating (arrows, Figs. 35, 36). Using TEM and X-ray diffraction in a separate study (Nelson et al., 1984), it was found that the surface coatings consist of finely-divided CaF_2 crystals only 4-15 nm in diameter, all packed loosely together. The thickness of the coatings produced by the APF gel and Duraphat varnish was approximately 0.2-0.3 micrometers whereas Fluor Protector produced coatings approximately 1 micrometer thick. Occasionally, large apatite-like crystals, sometimes 1 micrometer in length, were observed on the surface coatings (labelled Cr, Fig. 34).

Surface coatings produced by repeated APF applications (Bodde et al., 1985) followed by periods of remineralization were entirely different in morphology than those produced by a single APF application (Fig. 37). Not only was the surface coating much thicker but the individual CaF_2 single crystals, which ranged in size from 100-400 nm, were approximately twenty times larger than those produced by a single APF pre-treatment. Spherulites 1-4 micrometers in diameter could be observed on the outer surfaces of these coatings and they consisted of an agglomeration of apatite-like crystals approximately 0.1 micrometer in width and 1-2 micrometers long (Fig. 37).

The CaF_2 surface coatings produced by each of these topical fluoride agents could be removed by extraction with 1 $mol.l^{-1}$ KOH to reveal the underlying enamel surface. All three agents etched the enamel surface differently to produce their reaction product coatings. The APF gel selectively etched deep, tapered, pits 1-5 micrometers in diameter (Fig. 38) in rows of prisms parallel with the perikymata. Etching also occurred at the crystal level between the prism etch pits and small pores 0.1-0.3 micrometers in diameter could be seen in the enamel surface (Fig. 39). From these results we concluded that the effectiveness of an APF gel may be related to the possibility that CaF_2 particles in the deep prism etch pits would not be as easily washed away as CaF_2 particles on a smooth enamel surface and therefore act as a fluoride reservoir when the CaF_2 particles finally dissolve.

Conclusions

We have summarized several ways in which high resolution TEM and SEM have been used to solve dentally-related problems regarding surface morphology and crystallography of chemically modified enamel, dentin and apatite-ceramics. SEM evaluation of laser-treated enamel and dentin indicates considerable potential for the use of specific frequency laser radiation for dental applications. Electron microscopy techniques have been crucial in improving our understanding of many key physico-chemical processes that have been designed to alter the reactivity of dental enamel.

Acknowledgements

D.G.A. Nelson was supported by Medical Research Council of New Zealand project grant 85/121, and by a Fogarty International Research Fellowship F05 TW03162. Studies were also supported by NIH / NIDR grants DE07003 and DE05510.

References

Arends J, Nelson DGA, Dijkman AG, Jongebloed WL (1984) Effect of various fluorides on enamel structure and chemistry. In: Cariology Today, Int. Congr., Zurich, 1983, pp. 245-258. B Guggenheim (Ed.), Karger, Basel, Switzerland.

Bodde HE, Nelson DGA, Koops PG, Arends J (1985) Influence of repeated APF applications on long-term remineralization of initial lesions in bovine enamel. J Dent Res 64(1): 12-18.

Boyde A, Switsur VR, Fearnhead RW (1961) Application of the scanning electron probe X-ray microanalyzer to dental tissues. J Ultrastructure Res 5: 201-207.

Bres EF, Barry JC, Hutchinson JL (1984) A structural basis for the carious dissolution of the apatite crystals of human tooth enamel. Ultramicroscopy 12: 367-372.

Bres EF, Barry JC, Hutchinson JL (1985) High resolution electron microscope and computed images of human tooth enamel. J Ultrastructure Res 90: 261-274.

Brown WE, Smith JP, Lehr JR, Frazier AW (1962) Crystallographic and chemical relations between octacalcium phosphate and hydroxyapatite. Nature (London) 196: 1050-1055.

Brown WE, Schroeder LW, Ferris JS (1979) Interlayering of crystalline octacalcium phosphate and hydroxyapatite. J Phys Chem 83: 1385-1388.

Budz JA, LoRe M, Nancollas GH (1987) Hydroxyapatite and carbonated-apatite as models for the dissolution behavior of human dental enamel. Adv Dent Res 1: 314-321.

Cooper LF, Myers ML, Nelson DGA, Mowery AS (1988) Shear strength of composite resin bonded to laser pretreated dentin. J Prosth Dent 60: 45-49.

Figure 33. SEM of CaF_2 reaction product coating deposited on an enamel surface by neutral NaF varnish. Notice the two large globules.

Figure 34. SEM of CaF_2 reaction product coating deposited on an enamel surface by an acidic silane fluoride varnish. Notice the globules approximately 0.3 micrometers in diameter.

Figure 35. SEM of CaF_2 reaction product coating deposited on an enamel surface by neutral NaF varnish. Notice the very small CaF_2 particles (arrowed).

Figure 36. SEM of CaF_2 reaction product coating deposited on an enamel surface by an APF gel. Notice the very small CaF_2 particles (arrowed).

Figure 37. SEM of an enamel surface after repeated APF treatments. Rounded particles are single crystals of CaF_2, needle-like crystals are apatite.

Figure 38. SEM of a KOH-extracted enamel surface after having a single pre-treatment of an APF gel.

Figure 39. Higher magnification of Fig. 38.


33
1 µm

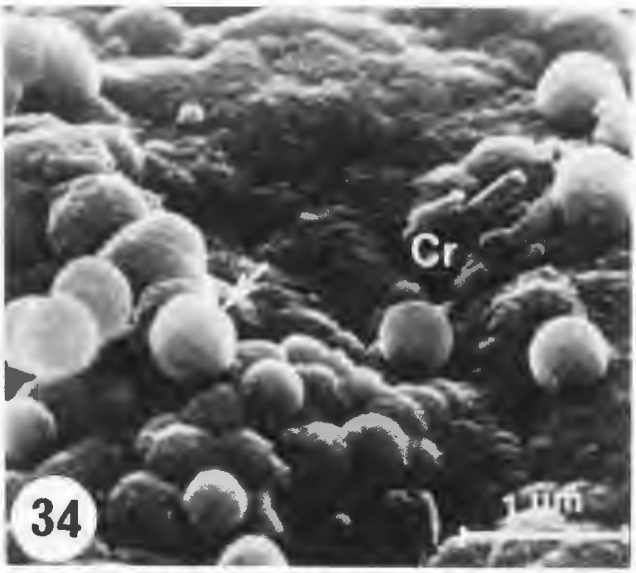
Cr
34
1µm


35
1µm

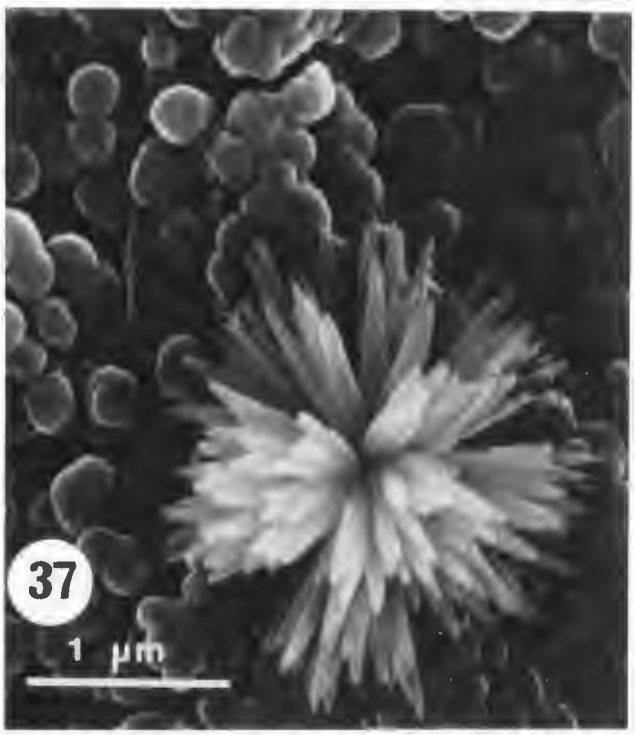
37
1 µm

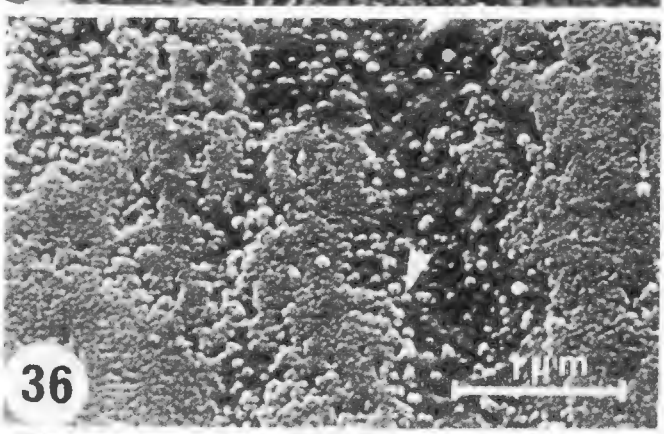
36
1µm


38
20µm

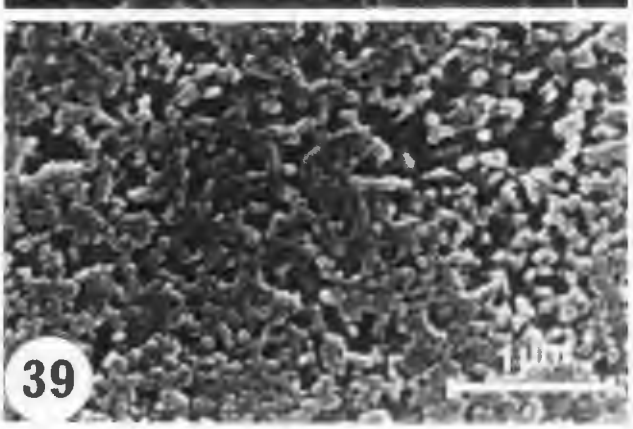
39
1µm

Ellies LG, Nelson DGA, Featherstone JDB (1988a) Crystallographic structure and surface morphology of sintered carbonated apatites. J Bio Materials Res 22: 541-553.

Ellies LG, Carter JM, Natiella JR, Featherstone JDB, Nelson DGA (1988b) Quantitative analysis of early in vivo tissue response to synthetic apatites. J Bio Materials Res 22: 137-148.

Elliott JC, Mackie PE, Young RA (1973) Monoclinic hydroxyapatite. Science 180: 1055-1057.

Featherstone JDB, Nelson DGA (1987) Laser effects on dental hard tissues. Adv Dent Res 1: 21-26.

Featherstone JDB, Shields CP, Khademazad B, Oldershaw MD (1983) Acid reactivity of carbonated-apatites with strontium and fluoride substitutions. J Dent Res 62: 1049-1053.

Featherstone JDB, O'Reilly MM, Shariati M, Brugler S (1986) Enhancement of remineralization in vitro and in vivo. In: Factors Relating to Demineralization and Remineralization of the Teeth, Leach SA (ed.), IRL Press, Oxford, U.K.

Frazier PD (1968) Adult human enamel - An EM study of crystallite size and morphology. J Ultrastruct Res 22: 1-11.

Gantt DG, Guntekunst MD (1988) The shape of enamel crystal within human enamel. J Dent Res 67:(special issue) 269, abstract 1255.

Glena R, Shields CP, Featherstone JDB, Cowles E (1984) Reactivity of carbonated-apatite in the presence of F and/or Sr. J Dent Res 63: 184, abstract 122.

Jones SJ, Boyde A (1987) Scanning microscopic observations on dental caries. Scanning Microscopy 1: 1991-2002.

Kautsky M (1988) Effect of salivary components on initial surface dissolution rates of ceramic carbonated apatites. MS Thesis, University of Rochester.

Kay MI, Young RA, Posner AS (1964) Crystal Structure of Hydroxyapatite. Nature 203: 1050-1053.

Kerebel B, Daculsi G, Kerebel LM (1979) Ultrastructural studies of enamel crystallites. J Dent Res 58(B): 844-850.

LeGeros RZ (1967) Crystallographic studies of the carbonate substitution in the apatite structure. Ph.D. Thesis, New York University, New York.

LeGeros RZ (1977) Apatites from aqueous and nonaqueous systems: Relation to biological apatites, First Int'l. Congress on Phosphorus Compounds, Rabat IMPHOS 199: 347-360.

Marshall AF, Lawless KR (1981) TEM study of the central dark line in enamel crystallites. J Dent Res 60: 1773-1782.

McLean JD, Nelson DGA (1982) High-resolution n-beam lattice images of hydroxyapatite. Micron 13: 409-413.

Nakahara H, Kakei M (1983) The central dark line in developing enamel crystallite: An electron microscopic study. Bull Josai Dent Univ 12: 1-7.

Nancollas GH, Tomazic B (1974) Growth of calcium phosphate on hydroxyapatite crystals. Effect of supersaturation and ionic medium. J Phys Chem 78: 2218-2225.

Nancollas GH (1982) Phase transformation during precipitation of calcium salts. In Dahlem Konferenzen 1982, GH Nancollas (ed), pp.79-99. Springer-Verlag, Berlin, West Germany.

Nelson DGA, McLean JD, Sanders JV (1983a) A high-resolution electron microscope study of synthetic and biological carbonated apatites. J Ultrastruct Res 84: 1-15.

Nelson DGA, Jongebloed WL, Arends J (1983b) Morphology of enamel surfaces treated with topical fluoride agents: SEM considerations. J Dent Res 62: 1201-1208.

Nelson DGA, Featherstone JDB, Duncan JF, Cutress TW (1983c) Effect of carbonate and fluoride on the dissolution behaviour of synthetic apatites. Caries Res 17: 200-211.

Nelson DGA, Jongebloed WL, Arends J (1984) Crystallographic structure of enamel surfaces treated with topical fluoride agents: TEM and XRD considerations. J Dent Res 63: 6-12.

Nelson DGA, McLean JD (1984a) High-resolution electron microscopy of octacalcium phosphate and its hydrolysis products. Calcif Tiss Int 36: 219-232.

Nelson DGA, McLean JD (1984b) Direct observation of near-atomic details in synthetic and biological apatite crystallites. In Tooth Enamel IV, RW Fearnhead, S Suga (eds.), pp. 47-51. Elsevier Science Publishers BV, Amsterdam, Netherlands.

Nelson DGA, Wood GJ, Barry JC, Featherstone JDB (1986a) The structure of (100) defects in carbonated apatite crystallites: A high resolution electron microscope study. Ultramicroscopy 19: 253-266.

Nelson DGA, Shariati M, Glena R, Shields CP, Featherstone JDB (1986b) Effect of pulsed low energy infrared laser irradiation on artificial caries-like lesion formation. Caries Res 20: 289-299.

Nelson DGA, Jongebloed WL, Featherstone JDB (1986c) Laser irradiation of human dental enamel and dentine. N Z Dent J 82: 74-77.

Nelson DGA, Wefel JS, Jongebloed WL, Featherstone JDB (1987) Morphology, histology and crystallography of human dental enamel treated with pulsed low energy IR laser radiation. Caries Res 21: 411-426.

Nelson DGA, Pearce EIF (1988) The application of backscattered electron imaging to demineralized enamel. J Dent Res 67:(special issue) 270, abstract 1260.

Nelson DGA, Barry JC, Shields CP, Glena R, Featherstone JDB (1989) Crystal morphology, composition and dissolution behaviour of carbonated apatites prepared at controlled pH and temperature. J Colloid Int Sci 130: 467-479.

Nylen MU, Eanes ED, Omnell K-A (1963) Crystal growth in rat enamel. J Cell Biol 18: 109-123.

Pearce EIF, Nelson DGA (1989) Microstructural features of carious enamel imaged with backscattered electrons. J Dent Res 68:113-118.

Rachinger WA, Phakey PP, Palamara J, Orams HJ (1982) Planar faults in dental hydroxyapatite. Calcif Tiss Int 34: 209-210.

Shellis RP, Hallsworth AS (1987) The use of scanning electron microscopy in studying enamel caries. Scanning Microscopy 1: 1109-1123.

Silverstone LM (1977) Remineralization phenomena. Caries Res 11 (suppl. 1): 59-84.

Simpson DR (1972) Problems of the composition and structure of the bone minerals. Clin Orthop Rel Res 86: 260-286.

Warshawsky H, Bai P, Nanci A (1987) Analysis of crystallite shape in rat incisor enamel. Anat Rec 218: 380-390.

Warshawsky H (1987) External shape of enamel crystals. Scanning Microscopy 1: 1913-1923.

Young RA (1974) Implications of atomic substitutions and other structural details in apatites. J Dent Res 53: 193-203.

Discussion with Reviewers

D.H. Pashley: In figure 9 which is a high magnification of a normal enamel surface, most of the enamel crystallites appear to have a diameter of about 50 nm. How much of this is sputtered coating and how much is crystal?
Authors: The sputter coating is approximately 10-12 nm thick, suggesting that the "true" diameter of the crystals is in the region of 30 nm.

D.H. Pashley: Does saliva inhibit acid dissolution of enamel by simply blocking intercrystalline channels, thereby decreasing the surface area of the enamel surface?
Authors: We do not believe that saliva inhibits acid dissolution of enamel by simply blocking intercrystalline channels, but that specific components of saliva adsorb onto enamel surfaces to form a pellicle.

D.H. Pashley: How many pulses of 50 J cm^{-2}, 1073 cm^{-1} laser energy are necessary to fuse an enamel or dentin smear layer to the underlying sound structure?
Authors: We routinely use 400 pulses for enamel and 20 pulses for dentin, but as little as 40 pulses for enamel and 10 pulses for dentin are effective.

D.H. Pashley: How much energy is lost in passing the laser light through fiberoptic bundles?
Authors: A suitable fiberoptic is not currently available for IR laser light of the frequencies used by us. It is necessary to use metal wave guides in laser devices presently marketed.

R.P. Shellis: With respect to the BSE work on carious lesions: Did you find that the prism peripheries were more highly mineralized than the prism cores in the body of the lesion for all types of lesions? Our findings (Shellis and Hallsworth, 1987) suggest that this phenomenon does not occur in at least some types of in vitro lesions.
Authors: Generally, in the body of the lesions, we found that the prism peripheries were more highly mineralized than the prism cores; although prisms in the surface layer and prisms near the advancing front of the lesion were often reversely mineralized. Also in the body of the lesions, striations of variable mineral density and spacing were observed often with the pattern duplicated almost exactly in adjacent prisms. Reasonably often, these striations are as highly mineralized as the prism peripheries.

R.P. Shellis: Have you examined your lased specimens after fracturing vertical to the surface, to see how deep the effect extends into the enamel?
Authors: Yes, we have examined vertical fracturing of lased enamel surfaces (Nelson et al., 1987). Fusion of enamel crystals extends to approximately 5 micrometers deep, whereas the effect on the organic component of enamel extends to 10-20 micrometers deep.

R.P. Shellis: The diphosphonate in the in vitro system you use to produce caries-like lesions appears to protect the surface enamel from dissolution very efficiently, so that the fused surfaces formed by lasing might be expected to retain their low permeability for a longer time than if diphosphonate were not present. Have you exposed lased specimens to diphosphonate-free in vitro caries systems or have you tried exposing them to the diphosphonate system for more than 12 hours?
Authors: In our more recent research we have used partially saturated buffers without diphosphonate and found similar results. Longer exposures to diphosphonate systems also have given similar conclusions.

H. Warshawsky: Having conceded that rhombohedral cut ends in enamel crystallites are not at variance with the hexagonal symmetry of apatite, how do you discount all the arguments raised by Warshawsky et al. (1987) that show that hexagonal crystals are incompatible with morphological observations, in particular their suggestion that the hexagonal shadows are two-dimensional projections of three-dimensional parallelepipeds?
Authors: This has already been answered in the text, but basically high resolution EM allows one to identify the crystallographic orientation of a crystal with respect to its morphology. We (and several others) have found that lattice images in projections parallel to the c-axis correspond precisely to the long axis of the needle-shaped apatite crystals and have flattened hexagonal outlines which must therefore be their true cross-sectional shape. The arguments raised by Warshawsky et al. (1987) do not relate the crystallographic orientation of apatite crystals to their morphology.

H. Warshawsky: Given a flattened hexagonal crystal that you believe the evidence firmly supports, why has no one ever seen the octagonal projections that one must predict would be seen when such crystals are viewed from an angle?
Authors: People have seen octagonal projections of apatite crystals which are in orientations not parallel to their c-axes. However, no one has ever seen an octagonal projection parallel to the c-axis, just hexagonal (60 or 120° angles) ones.

H. Warshawsky: If the central dark or light line seen in sectioned enamel crystallites is a crystallographic defect, why does it display Fresnel fringes? What other evidence do you have that the central dark or light line in these sectioned profiles corresponds to your light space between two plates of darker material as seen in figure 4?
Authors: The interface between any two materials (e.g., at grain boundaries) will produce Fresnel fringes. Hence, if the structure in the center of enamel crystals differs from the surrounding host material, then Fresnel fringes would be expected in TEM images of enamel crystals. At present, we have no physical evidence to prove that the planar defects seen in our synthetic apatite crystals are the same as the planar defects seen in enamel; although we believe they are related.

H. Warshawsky: The dark images on either side of the light space labeled PD in figure 4 display linear images that are also compatible with more interference patterns. What are the possibilities that the density changes are due to overlapping crystalline

plates and the lines are not fringes but Moire patterns?

Authors: Your explanation that this is due to two separate HAP crystals lying on a plate of octacalcium phosphate (OCP), although possible, would be statistically unlikely to occur very often. In our synthetic preparations these crystals are very common, and whatever they are, they cannot all be chance occurrences of three cyrstals lying on top of each other. Continuity of fringes across the crystal by itself does not prove the components are fused together, but the electron diffraction evidence and the computer simulation calculations by Nelson et al., (1986a) prove that the fringe pattern is not due to Moires from overlapping crystalline plates.

H. Warshawsky: How can you be sure that the fringes seen in figure 2 represent the orthorhombic symmetry of apatite in that orientation, rather than that of OCP as previously identified in the paper by Nelson, Salmi and Nancollas, J. Colloid and Interface Sc. 110: 32-39, 1986, figure 4c?

Authors: Image simulation calculations have shown a very good fit with hydroxyapatite (McLean and Nelson, 1982; Nelson et al. 1983a) in this orientation. In the OCP image you are referring to, the two-dimensional details in the image did not fit with HAP.